

# Solar-cycle variation of the rotational shear near the solar surface

A. Berekat<sup>1</sup>, J. Schou<sup>1</sup>, and L. Gizon<sup>1,2</sup>

<sup>1</sup> Max-Planck-Institut für Sonnensystemforschung, Justus-von-Liebig-Weg 3, 37077 Göttingen, Germany

<sup>2</sup> Institut für Astrophysik, Georg-August-Universität Göttingen, 37077 Göttingen, Germany

August 21, 2020

## ABSTRACT

**Context.** Helioseismology has revealed that the angular velocity of the Sun increases with depth in the outermost 35 Mm of the Sun. Recently, we have shown that the logarithmic radial gradient ( $d \ln \Omega / d \ln r$ ) in the upper 10 Mm is close to  $-1$  from the equator to  $60^\circ$  latitude.

**Aims.** We aim to measure the temporal variation of the rotational shear over solar cycle 23 and the rising phase of cycle 24 (1996-2015).

**Methods.** We used f mode frequency splitting data spanning 1996 to 2011 from the Michelson Doppler Imager (MDI) and 2010 to 2015 from the Helioseismic Magnetic Imager (HMI). In a first for such studies, the f mode frequency splitting data were obtained from 360-day time series. We used the same method as in our previous work for measuring  $d \ln \Omega / d \ln r$  from the equator to  $80^\circ$  latitude in the outer 13 Mm of the Sun. Then, we calculated the variation of the gradient at annual cadence relative to the average over 1996 to 2015.

**Results.** We found the rotational shear at low latitudes ( $0^\circ$  to  $30^\circ$ ) to vary in-phase with the solar activity, varying by  $\sim \pm 10\%$  over the period 1996 to 2015. At high latitudes ( $60^\circ$  to  $80^\circ$ ), we found rotational shear to vary in anti-phase with the solar activity. By comparing the radial gradient obtained from the splittings of the 360-day and the corresponding 72-day time series of HMI and MDI data, we suggest that the splittings obtained from the 72-day HMI time series suffer from systematic errors.

**Conclusions.** We provide a quantitative measurement of the temporal variation of the outer part of the near surface shear layer which may provide useful constraints on dynamo models and differential rotation theory.

**Key words.** Sun: Helioseismology – Sun: Interior – Sun: Rotation

## 1. Introduction

One of the major challenges in solar physics is to understand the physics behind the 11-year solar cycle. In many dynamo models, which attempt to explain the solar cycle, the differential rotation of the Sun plays an important role (see the reviews by Brandenburg & Subramanian (2005) and Charbonneau (2010)).

In an  $\alpha\Omega$  dynamo, rotational shear is responsible for the  $\Omega$ -effect which generates toroidal magnetic field from a poloidal magnetic field. The time variation of the shear has a direct influence on the magnetic field generation in the Sun as it may provide non-linear feedback on the dynamo mechanism (Küker et al. 1999). Additionally, the radial shear in the near-surface shear layer is a potential explanation for the equatorward migration of the activity belt during the solar cycle (Brandenburg 2005). Hence, providing quantitative information about the radial gradient of the rotation close to the surface of the Sun is indispensable. Measurements of the radial shear can also deliver constraints on differential rotation models (e.g., Kitchatinov & Rüdiger 2005). Kitchatinov (2016) recently related the near-surface shear to the subsurface magnetic field. Therefore, the time variation of the shear with the solar cycle may also help estimate the strength of the magnetic field below the surface at different phases of the cycle.

The radial shear can be measured by several helioseismic techniques; see Thompson et al. (1996), Schou et al. (1998), and the latest reviews of global and local helioseismology by Howe (2009) and Gizon et al. (2010), respectively.

Corbard & Thompson (2002) showed that the logarithmic radial gradient in the outer 16 Mm of the Sun is close to  $-1$  up to  $30^\circ$  latitude and becomes positive above  $55^\circ$  latitude. However, Berekat et al. (2014), hereafter BSG, found no indication of a change of sign at this latitude.

Antia et al. (2008) studied the time variation of the radial and latitudinal shear during solar cycle 23. They used 12 years (1996-2007) of p mode and f mode frequency splitting data from the Michelson Doppler Imager (MDI; Scherrer et al. 1995) on board the Solar and Heliospheric Observatory (SOHO). They also used 13 years (1995-2007) p mode frequency splitting data from the Global Oscillation Network Group (GONG). They applied a two-dimensional regularized least square method (Antia et al. 1998) for inferring the rotation rate. Then, they studied the time variation of both radial and latitudinal shears at several depths and latitudes. They found that the variation of the radial shear is about 20% of its average value at low latitudes at 14 Mm and below.

In this work, we investigate the solar cycle variation of the radial gradient of the rotation in the outer 13 Mm of the Sun using f modes. We use 19 consecutive years of frequency splitting data corresponding to the entire solar cycle 23 (1996-2010) and the rising phase of cycle 24 (2010-2015). These data are obtained from 360-day time series from the Medium- $l$  program of MDI and from the Helioseismic and Magnetic Imager (HMI; Schou et al. 2012) on board the Solar Dynamics Observatory. These data are different from what we used in BSG in which the splittings were obtained from 72-day time series. Therefore,

**Table 1.** Summary of 15 years of the MDI and five years (16-20) of the HMI data.

data set	starting date	$n$	$l$	$n_1$	$l_1$	$n_2$	$l_2$	$n_3$	$l_3$	$n_4$	$l_4$	$n_5$	$l_5$	$n_c$	$l_c$
1	1996.05.01	187	98	128	134	123	124	122	142	143	126	132	134	85	180
2	1997.04.26	182	104	120	133	129	135	126	136	128	131	129	121	83	175
3	1998.04.21	168	114	129	125	113	134	128	130	-	-	-	-	-	-
4	1999.04.16	160	111	132	127	134	133	127	135	127	135	128	127	86	164
5	2000.04.10	181	86	133	136	134	123	129	123	132	117	132	121	86	177
6	2001.04.05	177	108	127	126	124	147	133	113	132	127	122	140	76	191
7	2002.03.31	179	87	130	144	121	121	131	137	129	144	130	124	83	181
8	2003.03.26	179	103	125	140	119	144	134	133	116	124	131	111	79	176
9	2004.03.20	178	96	119	138	124	138	126	116	119	146	131	129	70	180
10	2005.03.15	178	106	131	134	129	135	128	127	128	118	124	132	75	180
11	2006.03.10	173	95	132	137	126	134	133	127	123	119	131	130	77	166
12	2007.03.05	177	106	137	130	125	121	130	132	124	139	126	123	80	175
13	2008.02.28	184	96	132	125	135	118	140	120	137	141	123	134	79	174
14	2009.02.22	183	91	140	135	131	122	127	141	126	136	125	118	70	172
15	2010.02.17	163	128	135	134	138	136	126	139	128	133	113	138	84	164
16	2010.04.30	149	131	119	132	115	139	125	123	120	157	109	144	74	173
17	2011.04.25	152	118	119	127	116	135	122	140	120	136	127	133	79	184
18	2012.04.19	152	110	115	144	116	131	117	137	114	130	108	161	70	196
19	2013.04.14	166	100	125	128	118	147	124	140	124	141	118	134	77	171
20	2014.04.09	173	103	119	149	122	149	114	138	126	125	119	142	75	180

**Notes.** The number of splitting frequencies available in each data set is given by  $n$  and  $n_1$  to  $n_5$  are the constituent 72-day time series. The minimum angular degree recovered is given by  $l$  in each set.  $n_c$  and  $l_c$  represent similar quantities for the common modes between each 360-day and the corresponding 72-day data sets. For details see Sect. 4.1.

we compare the gradient obtained from these two different data sets in Sect. 4.1 before we investigate the time variation of the gradient in Sect. 4.2.

## 2. Observational data

We consider only f modes. We denote mode frequency by  $\nu_{lm}$  where  $l$  and  $m$  are the spherical harmonic degree and for azimuthal order, respectively. We use 18 odd  $a$ -coefficients for each  $l$  (Schou et al. 1994) obtained from MDI and HMI data, which are defined by

$$\nu_{lm} = \nu_l + \sum_{j=1}^{36} a_{l,j} \mathcal{P}_j^{(l)}(m), \quad (1)$$

where  $\nu_l$  is the mean multiplet frequency, and  $\mathcal{P}_j^{(l)}$  are orthogonal polynomials of degree  $j$ . We use two sets of data of each instrument; the  $a$ -coefficients which are obtained from 72-day and 360-day time series, resulting in four data sets:

- MDI360: 15 sets obtained from 360-day MDI (1996-2011)
- HMI360: 5 sets obtained from 360-day HMI (2010-2015)
- MDI72: 74 sets obtained from 72-day MDI (1996-2011)
- HMI72: 25 sets obtained from 72-day HMI (2010-2015).

We summarize the number of modes found in each data set in Table 1. The differences between the splittings obtained from 360-day and 72-day time series of MDI data were investigated in great detail by Larson & Schou (2015), who also provide further details on the analysis.

The MDI72 and HMI72 are used only for the comparison between the results obtained from these data sets and the corresponding results obtained from data sets MDI360 and HMI360. We note here that each 360-day time series is the combination of the five corresponding 72-day ones except for the third data set

in Table 1, which was made from three non-consecutive 72 day time series (Larson & Schou 2015) because of problems with the SOHO spacecraft.

## 3. Method

Our method for measuring the radial gradient is identical to the one used by BSG. We explain our method here succinctly and refer the reader to BSG for detailed explanation. We model the rotation rate as changing linearly with depth

$$\Omega(r, u) = \Omega_0(u) + (1 - r)\Omega_1(u), \quad (2)$$

where  $r$  is the distance to the center of the Sun normalized by its photospheric radius ( $R_\odot$ ),  $u$  is the cosine of co-latitude and,  $\Omega_0(u)$  and  $\Omega_1(u)$  are the rotation rate at the surface and the slope, respectively. Then, we perform a forward problem using the relation between the  $a$ -coefficients and  $\Omega$  which is given by

$$2\pi a_{l,2s+1} = \int_0^1 dr \int_{-1}^1 du K_{ls}(r, u) \Omega(r, u), \quad (3)$$

where  $K_{ls}$  are kernels. We obtain

$$\tilde{\Omega}_{ls} \equiv \frac{2\pi a_{l,2s+1}}{\beta_{ls}} = \langle \Omega_0 \rangle_s + (1 - \bar{r}_{ls}) \langle \Omega_1 \rangle_s, \quad (4)$$

where the  $\beta_{ls}$  are the total integrals of the radial component of the kernels (see Eq.(4) in BSG) and  $\bar{r}_{ls}$  is the central of gravity of the radial kernels. The  $\langle \rangle$  denotes latitudinal averages. Next, we perform an error-weighted least square fit of  $\tilde{\Omega}_{ls}/2\pi$  versus  $(1 - \bar{r}_{ls})$  to determine  $\langle \Omega_0 \rangle_s$  and  $\langle \Omega_1 \rangle_s$  for each data set.

In the last step of our analysis, we apply the inversion method used by Schou (1999) to  $\langle \Omega_0 \rangle_s$  and  $\langle \Omega_1 \rangle_s$  to infer the rotation rate at each target latitude  $u_0$  and from this obtain  $d \ln \Omega / d \ln r$ .

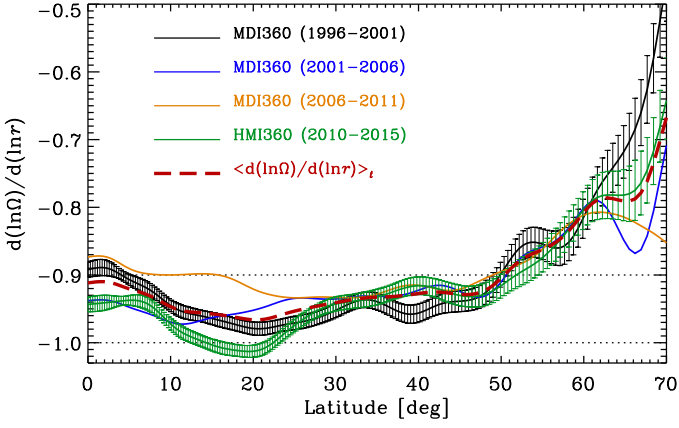


**Fig. 1.** Time average of the logarithmic radial gradient versus target latitude. Black, blue, and orange lines represent each consecutive five year time average of  $d \ln \Omega / d \ln r$  obtained from MDI360. The green line shows the same quantity obtained from HMI360. The red dashed line shows the 19 year (1996-2015) time average of  $d \ln \Omega / d \ln r$ . The error bars are  $1\sigma$ . The errors on the orange and blue lines are similar to the black one. The errors on the red dashed line are similar to the thickness of the line.

**Table 2.** Selected values of 19 year (1996-2015) time averaged values of the logarithmic radial gradient from Fig. 1.

Latitude	$\langle d \ln \Omega / d \ln r \rangle_t$
0°	$-0.912 \pm 0.004$
10°	$-0.947 \pm 0.003$
20°	$-0.966 \pm 0.004$
30°	$-0.941 \pm 0.004$
40°	$-0.927 \pm 0.005$
50°	$-0.906 \pm 0.007$
60°	$-0.809 \pm 0.011$

## 4. Results

Figure 1 shows the radial gradient obtained from the MDI360 and the HMI360 data sets. Also shown in Fig. 1 and summarized in Table 2 is the value of the 19 year (1996-2015) time average of  $d \ln \Omega / d \ln r$ . Going from the equator, this average fluctuates between  $-0.97$  and  $-0.9$  up to  $50^\circ$  latitude, above which it steadily increases with latitude. We included data sets 15 and 16 in the average even though they have 288 days of overlap.

Figure 1 also shows consecutive five year time averages of  $d \ln \Omega / d \ln r$  which roughly represent different phases of two solar cycles. There is evidence of the solar cycle variation of  $d \ln \Omega / d \ln r$  at low and high latitudes. These results lead us to investigate the temporal variation of  $d \ln \Omega / d \ln r$  with annual cadence. We show the results in Sect. 4.2.

We note that the time averaged value obtained from the HMI360 data set does not show the same trend as the one measured in BSG above  $60^\circ$  latitude using the first 20 sets of HMI72 (see Fig. 3 of BSG). We explore the difference between our results and BSG of each instrument in detail in the next section.

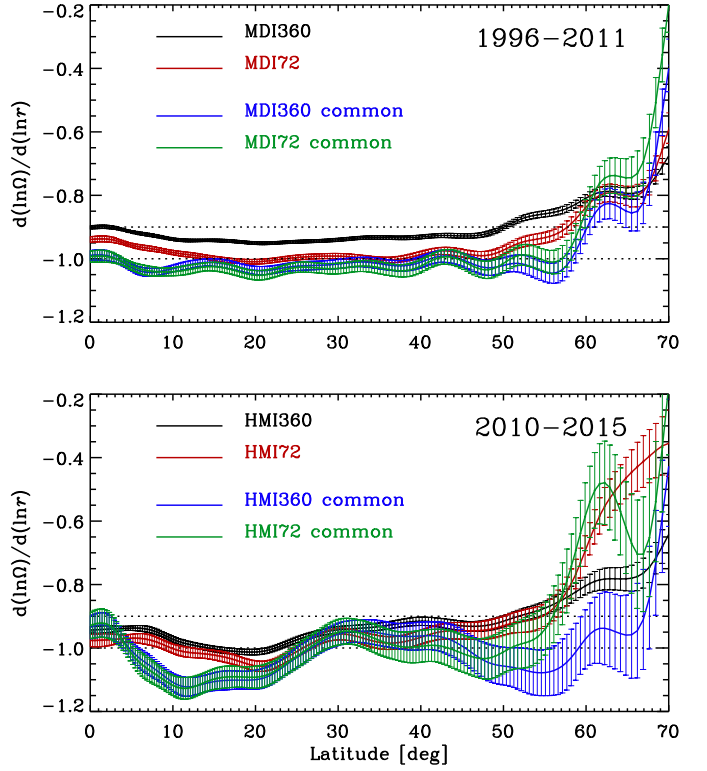


**Fig. 2.** Comparison of time averages of  $d \ln \Omega / d \ln r$  versus target latitude using 15 years of MDI data (upper panel) and five years of HMI data (lower panel). In both panels, black and blue lines show results obtained from splittings from 360-day time series of all and common modes (see, Sect. 4.1), respectively. The red and green lines show the results obtained from 72-day time series of all and common modes, respectively. The dotted lines mark the constant values of  $-0.9$  and  $-1$  at all latitudes. The error bars are  $1\sigma$ .

### 4.1. Results obtained from 72-day vs. 360-day data

In this section, we compare the radial gradient derived from splittings obtained from 360-day time series and 72-day time series from both MDI and HMI. First, we show the results of MDI data and then HMI.

The first panel of Fig. 2 shows the 15 year (1996-2011) time average of the radial gradient obtained from data sets MDI360 and MDI72. The result from data set MDI72 is identical to the MDI result found by BSG. For the MDI data, the absolute value of  $d \ln \Omega / d \ln r$  is about 5% smaller than the values found by BSG. This difference can be explained by the fact that using MDI360 and HMI360 data sets enables us to probe roughly 3 Mm deeper than using data sets MDI72 and HMI72. As a consequence,  $\bar{\Omega}_{l0} / 2\pi$  is not linear in  $r$  any more, as shown in Fig. 3, which in turn means that the fitted values depend on the modes included.

The maximum value of  $l = 300$  is the same for all data sets, but the minimum value of  $l$  is different; see Table 1. Therefore, we compare the results obtained from each set in MDI360 with those from the corresponding five sets of MDI72, using only the common modes. The result is shown in the first panel of Fig. 2. For this comparison we excluded the last data set of MDI72 because it is after the last set in MDI360. Considering only common modes causes us to exclude more than half of the modes

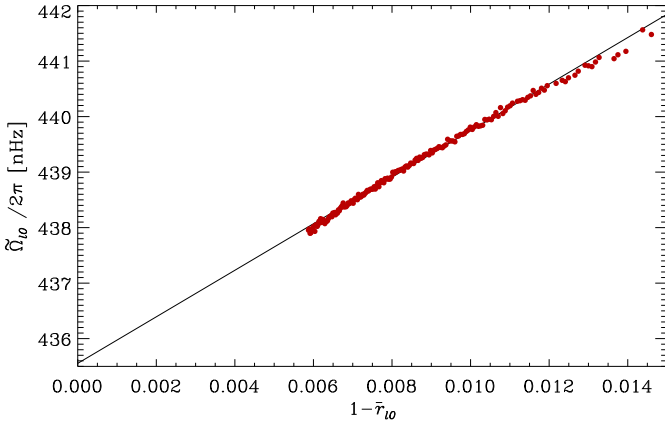


**Fig. 3.**  $\tilde{\Omega}_{10}/2\pi$  versus  $(1-\bar{\tau}_{10})$  obtained from the data set starting 10 April 2000 of MDI360. The black line is the error weighted linear least square fit. We avoid plotting the error bars as they are in similar size of the symbols.

from each data set in MDI360 (see last column of Table 1). The difference between the results obtained from MDI360 and MDI72 are reduced substantially and they are now in agreement to better than  $1\sigma$  up to  $50^\circ$  latitude. This difference increases gradually toward higher latitudes which shows that the results above  $50^\circ$  latitude are not reliable. We note that one would expect the results to be consistent to better than  $1\sigma$ , as they are obtained from the same underlying data. Thus there is clear evidence that the splitting data suffer from systematic errors.

We applied the same comparison to sets HMI360 and HMI72. The five year time averages from using both all and only the common modes are shown in the bottom panel of Fig. 2. There is a significant discrepancy between the two results obtained from sets HMI360 and HMI72 above  $60^\circ$  latitude which does not disappear even when comparing the results obtained from the common modes. This shows that the HMI data are even more affected by systematic errors than the MDI data.

For HMI data, we carry out further analysis by comparing the results derived from common modes of each year. Except for the first and last year the difference between the results persists. The perfect agreement of the results in the last year encourage us to compare common modes between these two data sets. This comparison shows that the difference between  $a_3$  and  $a_5$  of those data sets are significant. In average, the values of  $a_3$  of HMI360 is larger and  $a_5$  is smaller than the corresponding HMI72 ones by about  $3\sigma$ . There are also clear systematic errors in those coefficients with larger discrepancies in the earlier than in the later years.

Unfortunately, these comparisons do not tell us what causes the systematic errors or how to correct them. Understanding this will require a more detailed analysis (Larson & Schou in prep.). However, our results suggest that HMI72 suffer from systematic errors as the results obtained using HMI360 are not significantly different from the results of data sets MDI360 and MDI72. Moreover, we expect that the splittings obtained from longer time series have better quality as the peaks are better resolved. (Larson & Schou 2015).

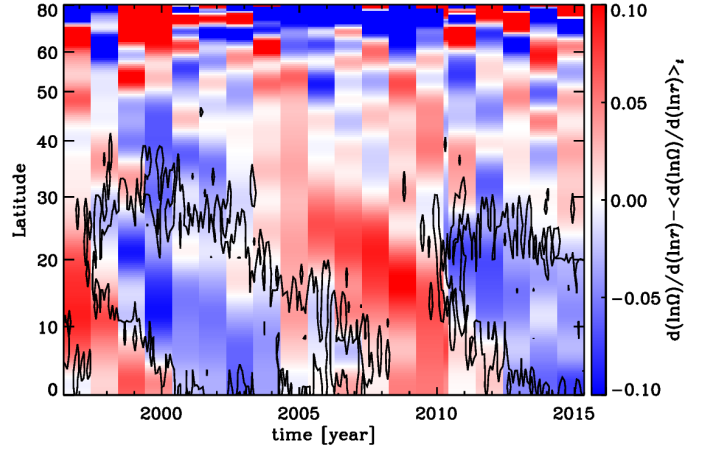


**Fig. 4.** Time variation of  $d \ln \Omega / d \ln r$  relative to its 19 year time average. The thin stripe in the plot shows the result obtained from data set 15 overlapped on data set 16 as there is 288 days overlap between these two data sets. The contours show the two hemisphere averaged butterfly diagram of the sunspot area of 5 per millionths of a hemisphere (courtesy of D. Hathaway; see <http://solarscience.msfc.nasa.gov/greenwch.shtml>).

#### 4.2. Solar cycle variation of the radial gradient

We measure the variation of  $d \ln \Omega / d \ln r$  relative to its time averaged value from 1996 to 2015 using data sets MDI360 and HMI360. We show the results in Fig. 4 together with the butterfly diagram. These measurements reveal two cyclic patterns; one at low latitudes from the equator to about  $40^\circ$  latitude and one above  $60^\circ$  latitude. There is no clear signal between about  $40^\circ$  and  $60^\circ$  latitude.

Below  $40^\circ$ , there exist bands where the rotation gradient is about 10% larger and smaller than the average. As illustrated by the butterfly diagram in Figure 4, the band with steeper than average gradient (blue in Fig. 4) follows the activity belt quite closely. These bands are also similar to the torsional oscillation signal (see, e.g., Howe et al. (2006); Antia et al. (2008))

The temporal variation of  $d \ln \Omega / d \ln r$  at high latitudes is more than 10% of its average value and has the opposite behavior to that at low latitudes. However, as we pointed out earlier the measured values of the gradient above  $50^\circ$  latitude are not reliable, so any results here have to be interpreted with caution.

The statistical significance of these signals is shown in Fig. 5 and the standard deviation in time and the time averaged errors in Fig. 6. The measured signals are statistically significant at low and high latitudes as they are at the 3 to  $8\sigma$  level, while they are indeed not significant between  $40^\circ$  and  $60^\circ$  latitude.

We note here that the results obtained from MDI360 and HMI360 are only different by about 1% when using modes with  $l \geq 120$ , corresponding roughly to the range used by the 72-day analysis and over which the rotation rate changes linearly with depth.

It is well known that the phase and amplitude of the solar cycle variations of the rotation rate vary with depth and latitude (Vorontsov et al. 2002; Basu & Antia 2003; Howe et al. 2005; Antia et al. 2008), but the temporal variation of the gradient has not been previously reported over the same depth range as used in this work.

Antia et al. (2008) found a similar pattern with similar amplitude of the temporal variation of the radial gradient at  $0.98R_\odot$  as ours. They used the first eight odd  $a$ -coefficients obtained



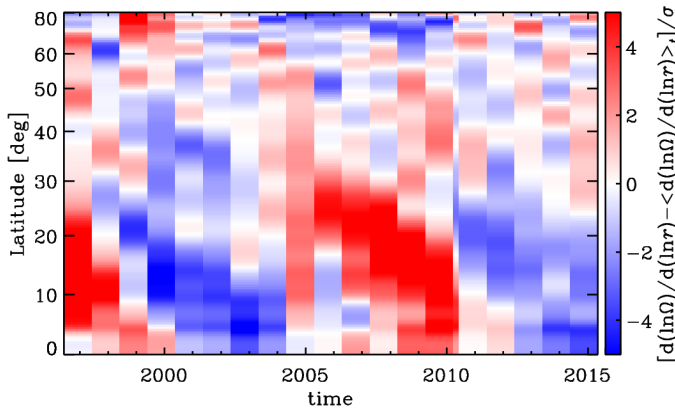


**Fig. 5.** Statistical significance in change of  $d \ln \Omega / d \ln r$  relative to its average values at different latitudes and time.  $\sigma$  is the error on  $d \ln \Omega / d \ln r$  of each year.

from MDI p and f modes and GONG p modes spanning 1995 to 2007. Despite the similarity in pattern and amplitude, the sign of the change in the gradient of their results is opposite to ours. They saw that sunspots occurred where the absolute value of the gradient is smaller than the average value which is the opposite of what we see. This difference might come from the fact that we are measuring the temporal variation around  $0.99R_{\odot}$  while they measured it at  $0.98R_{\odot}$ . We also note that Antia et al. (2008) used the earlier version of the MDI data (see Larson & Schou (2015) and BSG) which might explain the discrepancy that Antia et al. (2008) saw between GONG and MDI data at  $0.98R_{\odot}$  and shallower layers.

## 5. Conclusion

We make measurements of the radial gradient over 19 years (1996-2015) corresponding to solar cycle 23 and the rising phase of cycle 24 in the outer 13 Mm of the Sun. We use recently available f mode frequency splittings data obtained from 360-day time series of MDI spanning 1996 to 2011 and HMI spanning 2010 to 2015. The values of the radial gradient derived from MDI360 and HMI360 fluctuate between  $-0.97$  and  $-0.9$  up to  $50^{\circ}$  latitude. These values are a few percent larger than measured values by BSG which are obtained from MDI72 and HMI72. It turns out that this difference comes from the fact that the angular velocity does not change linearly with depth to deeper than about 10 Mm below the surface.

We also compare the radial gradient obtained from common modes of two different data sets of each instrument. These comparisons reveal that the measured values of  $d \ln \Omega / d \ln r$  above  $50^{\circ}$  latitude are not reliable. Another important finding is that there are considerable systematic errors in HMI data that needs further investigation.

By measuring the variation of rotational shear relative to its 19 year time averaged value we find two cyclic patterns at low ( $0^{\circ}$  to  $30^{\circ}$ ) and at high ( $60^{\circ}$  to  $80^{\circ}$ ) latitudes with similar period of the solar cycle. Both patterns show bands of larger and smaller than average shear moving toward the equator and poles at low and high latitudes, respectively. The relative change in the shear is about 10% at low latitudes and 20% at high latitudes. Although the values of  $d \ln \Omega / d \ln r$  above  $50^{\circ}$  are not reliable, the temporal variation of  $d \ln \Omega / d \ln r$  is significant above  $60^{\circ}$  latitudes. This finding may have important implications for dy-

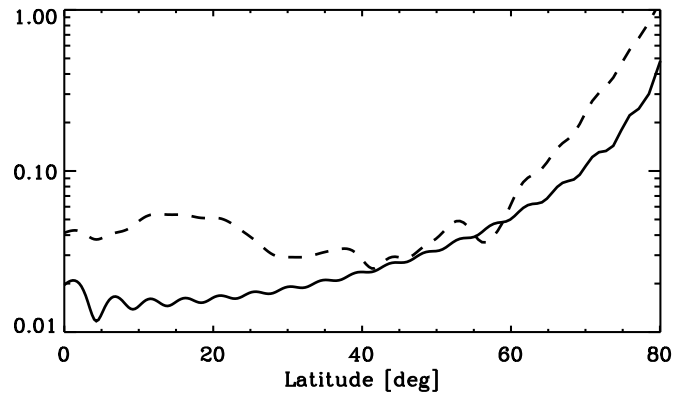


**Fig. 6.** Comparison between the standard deviation of the time variation of the radial shear relative to its time averaged value (dashed line) and the time averaged error of the shear (solid line) obtained from data sets MDI360 and HMI360.

namo models as this variation is considerable compared to the torsional oscillation (Antia et al. 2008).

The cyclic behavior of the shear at low latitudes agrees with the recent theoretical work by Kitchatinov (2016) who showed that the strength of the shear increases because of the presence of the strong magnetic field. Therefore accurate measurements of the shear might be a way of determining of the sub-surface magnetic field.

*Acknowledgements.* We thank T. P. Larson for discussions regarding details of the HMI data, and A. Birch for various discussions and his useful comments about the paper. L. Gizon acknowledges support from the Center for Space Science at the NYU Abu Dhabi Institute. SOHO is a project of international cooperation between ESA and NASA. The HMI data are courtesy of NASA/SDO and the HMI science team.

## References

- Antia, H. M., Basu, S., & Chitre, S. M. 1998, MNRAS, 298, 543
- Antia, H. M., Basu, S., & Chitre, S. M. 2008, ApJ, 681, 680
- Barekat, A., Schou, J., & Gizon, L. 2014, A&A, 570, L12
- Basu, S. & Antia, H. M. 2003, ApJ, 585, 553
- Brandenburg, A. 2005, ApJ, 625, 539
- Brandenburg, A. & Subramanian, K. 2005, Phys. Rep., 417, 1
- Charbonneau, P. 2010, Living Reviews in Solar Physics, 7, 3
- Corbard, T. & Thompson, M. J. 2002, Sol. Phys., 205, 211
- Gizon, L., Birch, A. C., & Spruit, H. C. 2010, ARA&A, 48, 289
- Howe, R. 2009, Living Reviews in Solar Physics, 6
- Howe, R., Christensen-Dalsgaard, J., Hill, F., et al. 2005, ApJ, 634, 1405
- Howe, R., Komm, R., Hill, F., et al. 2006, Sol. Phys., 235, 1
- Kitchatinov, L. L. 2016, Astronomy Letters, 42, 339
- Kitchatinov, L. L. & Rüdiger, G. 2005, Astronomische Nachrichten, 326, 379
- Küker, M., Arlt, R., & Rüdiger, G. 1999, A&A, 343, 977
- Larson, T. P. & Schou, J. 2015, Sol. Phys., 290, 3221
- Scherrer, P. H., Bogart, R. S., Bush, R. I., et al. 1995, Sol. Phys., 162, 129
- Schou, J. 1999, ApJ, 523, L181
- Schou, J., Antia, H. M., Basu, S., et al. 1998, ApJ, 505, 390
- Schou, J., Christensen-Dalsgaard, J., & Thompson, M. J. 1994, ApJ, 433, 389
- Schou, J., Scherrer, P. H., Bush, R. I., et al. 2012, Sol. Phys., 275, 229
- Thompson, M. J., Toomre, J., Anderson, E. R., et al. 1996, Science, 272, 1300
- Vorontsov, S. V., Christensen-Dalsgaard, J., Schou, J., Strakhov, V. N., & Thompson, M. J. 2002, Science, 296, 101